

Supporting Information

Aqueous ROPISA of α -aminoacid *N*-carboxyanhydrides: polypeptide block secondary structure influences nanoparticle shape anisotropy

Chloé Grazon,^{‡abc} Pedro Salas-Ambrosio,^{‡a} Segolene Antoine,^a Emmanuel Ibarboure,^a Olivier Sandre,^a Andrew J. Clulow,^{d,e} Ben J. Boyd,^{d,f} Mark W. Grinstaff,^b Sébastien Lecommandoux,^{*a} Colin Bonduelle.^{*a}

^a Univ. Bordeaux, CNRS, Bordeaux INP, LCPO, UMR 5629, F-33600, Pessac, France.

^b Departments of Chemistry and Biomedical Engineering, Boston University, Boston, MA (USA)

^c Univ. Bordeaux, Institut des Sciences Moléculaires (CNRS UMR 5255), 33405 Talence, France.

^d Drug Delivery, Disposition and Dynamics, Monash Institute of Pharmaceutical Sciences, 381 Royal Parade, Parkville, VIC 3052, Australia

^e Australian Synchrotron, ANSTO, 800 Blackburn Road, Clayton, VIC 3168, Australia

^f ARC Centre of Excellence in Convergent Bionano Science and Technology, Monash Institute of Pharmaceutical Sciences, 381 Royal Parade, Parkville, VIC 3052, Australia

[‡] co-first authors

Summary

Figure S1-2: SEC of copolymers PEG- <i>b</i> -PBLG and PEG- <i>b</i> -PLEu	2
Figure S3-S6: ¹ H NMR copolymer PEG- <i>b</i> -PBLG	2
Figure S7-S10: ¹ H NMR copolymer PEG- <i>b</i> -PLEu	3
Figure S11: AFM images	7
Figure S12: Photos of bluish solutions upon ROPISA	7
Figure S13: polypeptides nanoparticles SAXS profiles and fits	9
Table S1: Values calculated from the fits using the cylinder model in SAXS analyses	9
Figure S14: Diameter size distribution from TEM imaging	10
Figure S15: PEG- <i>b</i> -PBLDG ₁₀ : ¹ H NMR, SEC, FTIR and TEM characterization	11

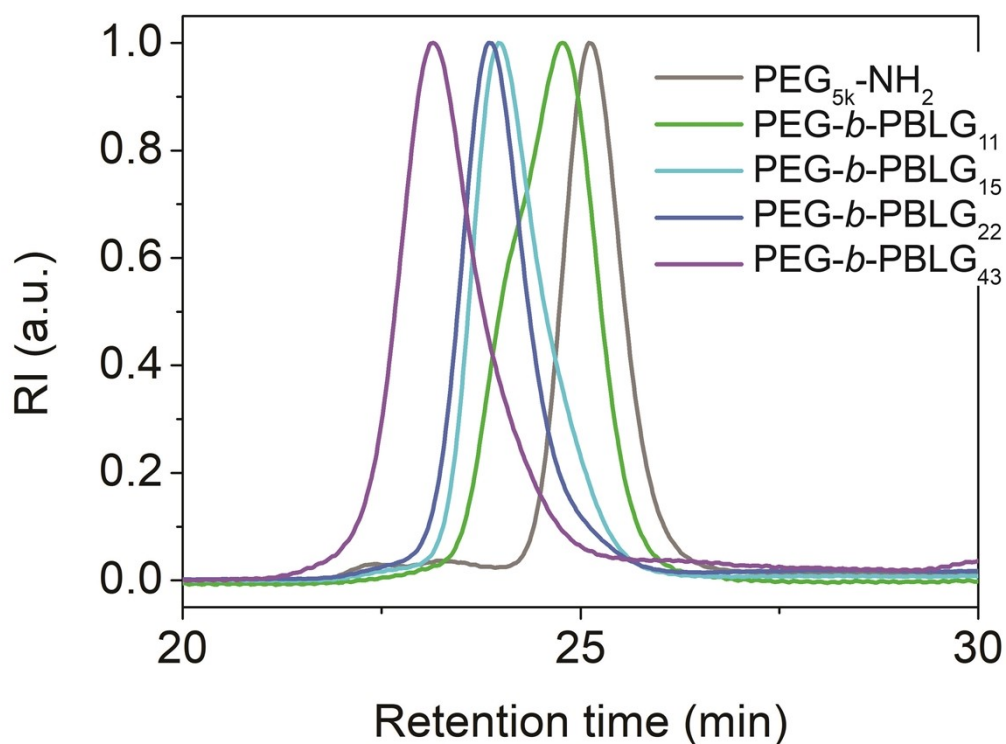


Figure S1. Steric exclusion chromatograms of copolymer **PEG-*b*-PBLG** analyzed in DMF (+ 1g·mL⁻¹ LiBr)

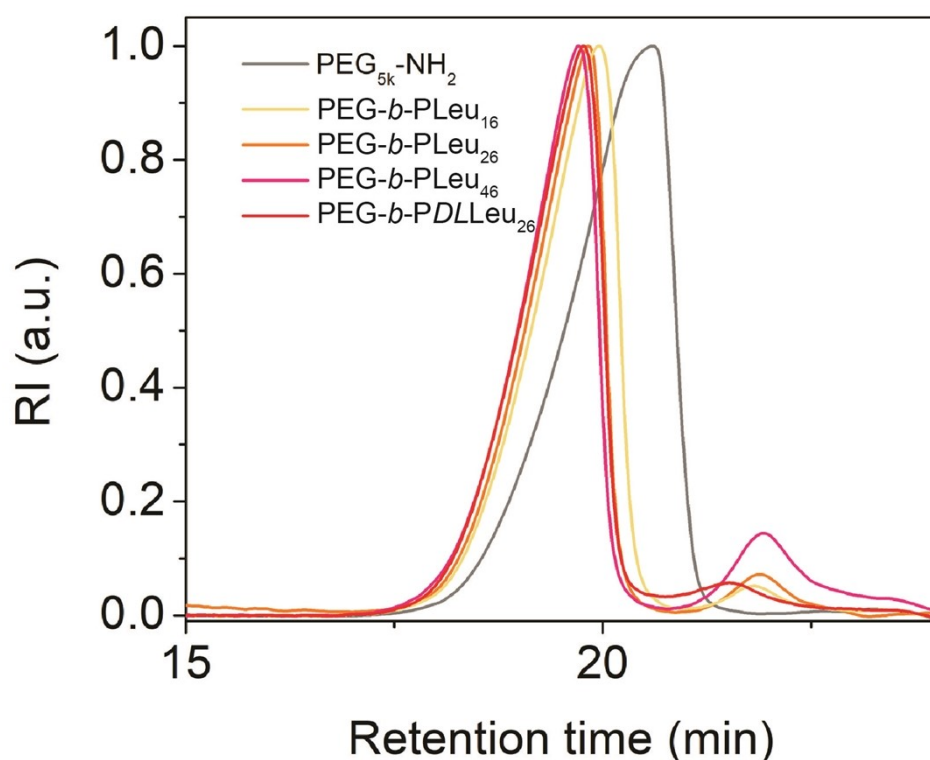


Figure S2. SEC chromatograms of **PEG-*b*-PLeu** analyzed in HFIP.

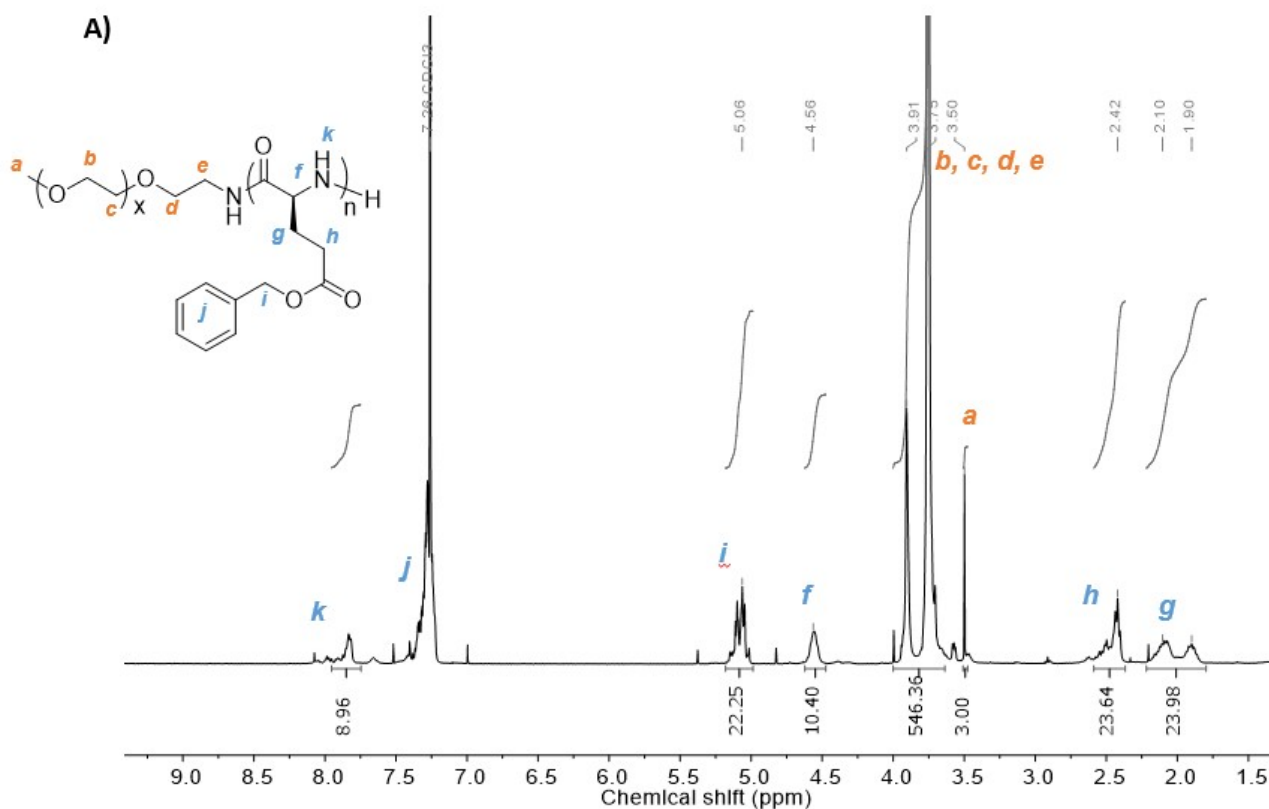


Figure S3. ¹H NMR of PEG-*b*-PBLG₁₁ in CDCl₃ with TFA 15%

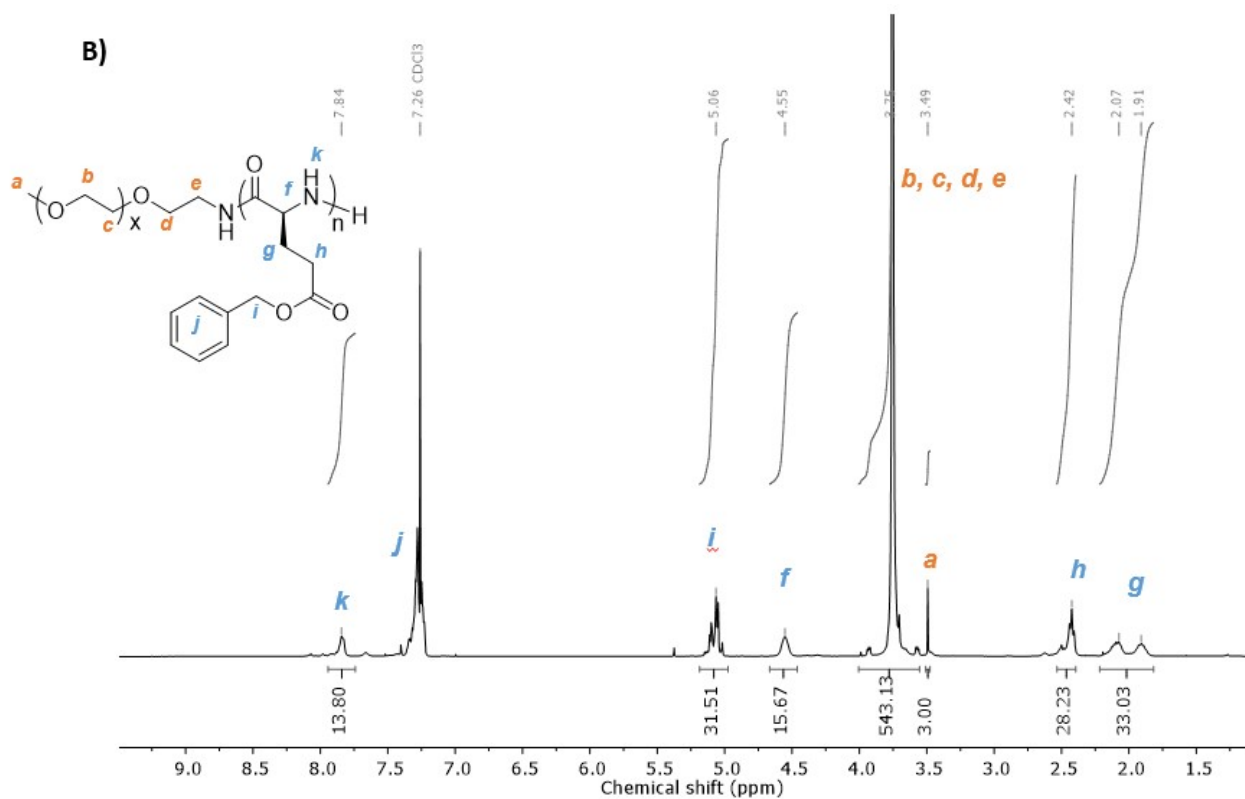


Figure S4. ¹H NMR of PEG-*b*-PBLG₁₅ in CDCl₃ with TFA 15%

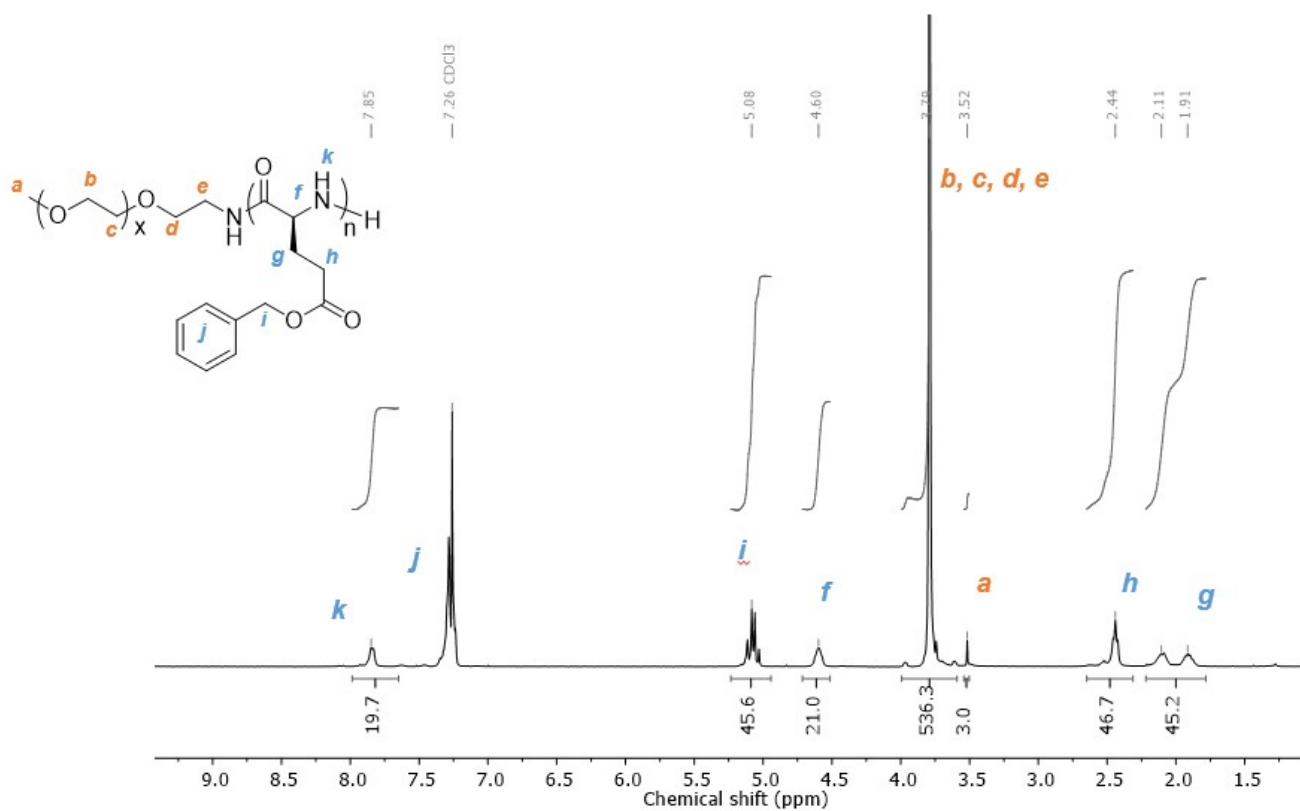


Figure S5. ¹H NMR of PEG-*b*-PBLG₂₂ in CDCl₃ with TFA 15%

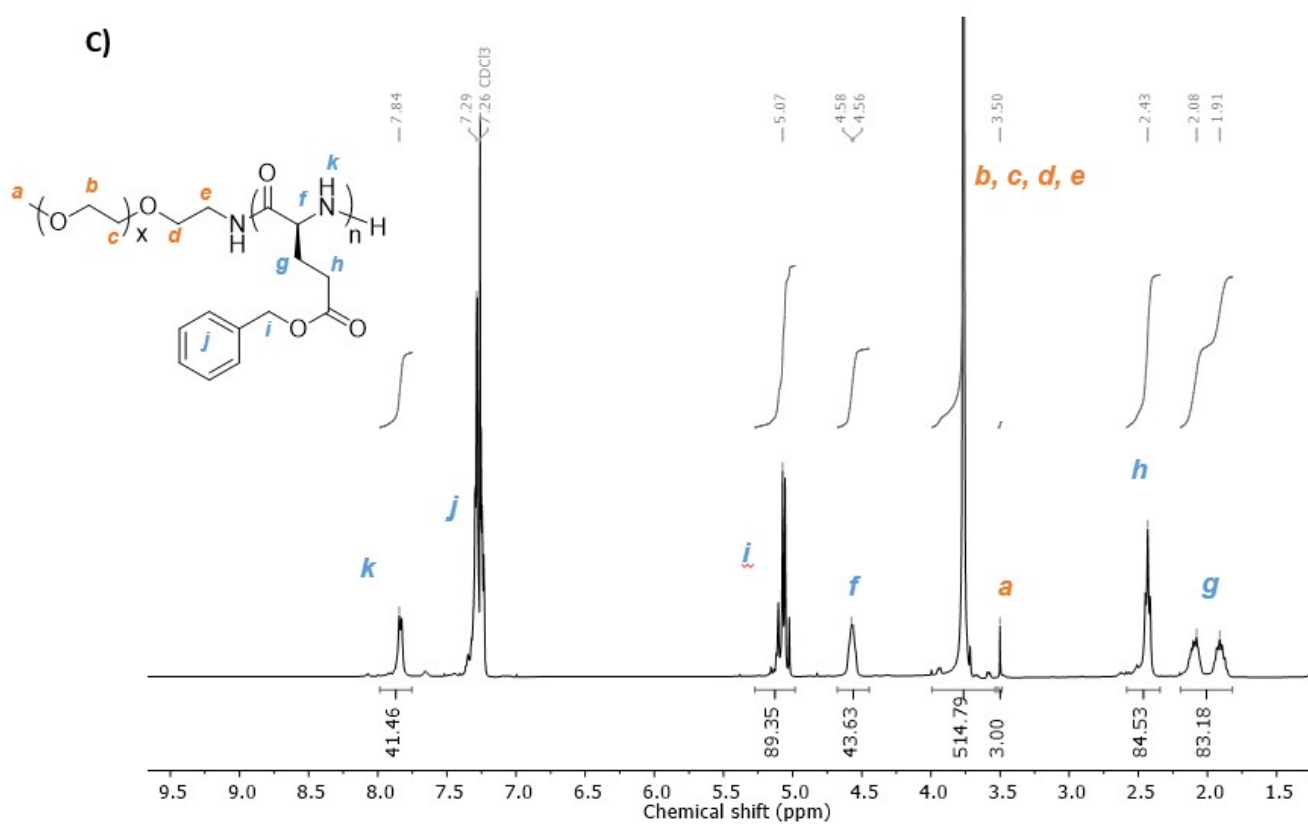
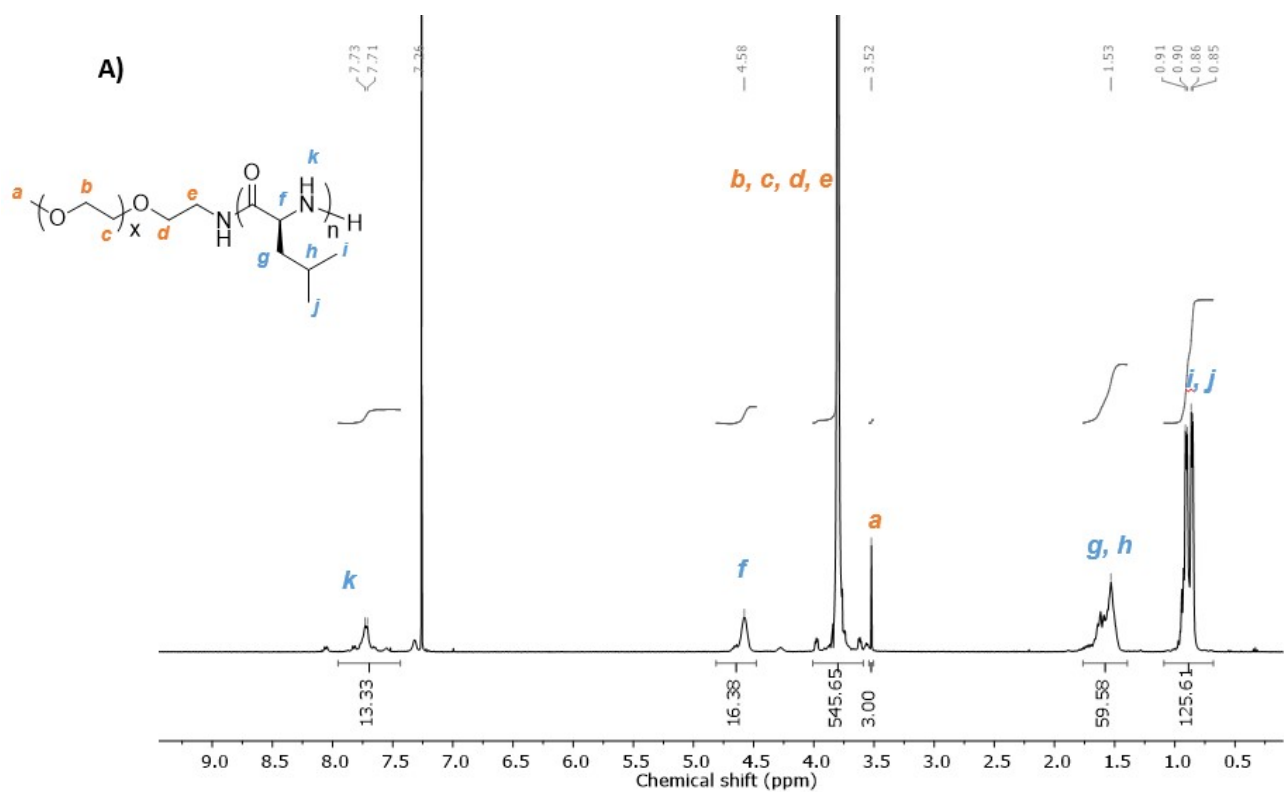


Figure S6. ¹H NMR of PEG-*b*-PBLG₄₃ in CDCl₃ with TFA 15%



F

figure S7. ¹H NMR of PEG-*b*-PLeu₁₆ in CDCl₃ with TFA 30%

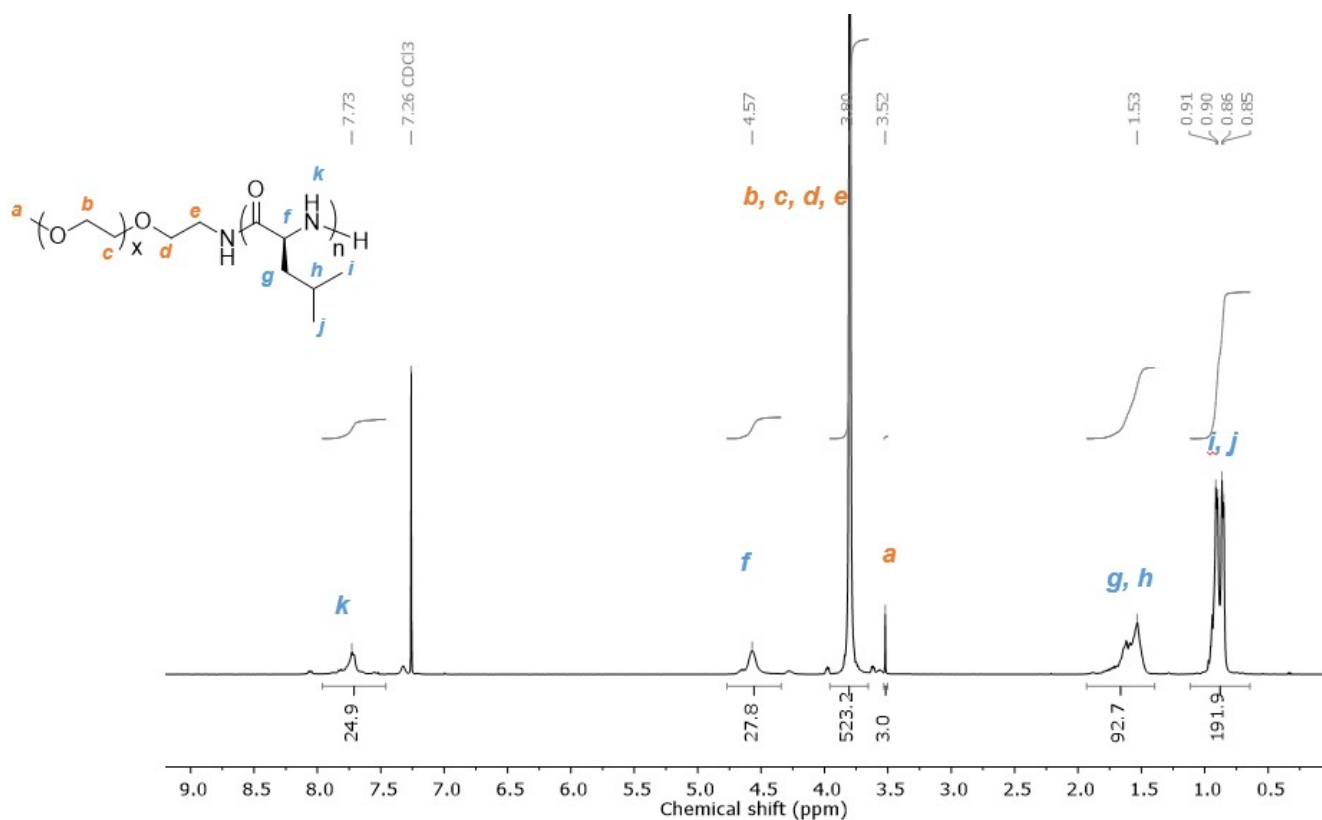


Figure S8. ¹H NMR of PEG-*b*-PLeu₂₆ in CDCl₃ with TFA 30%

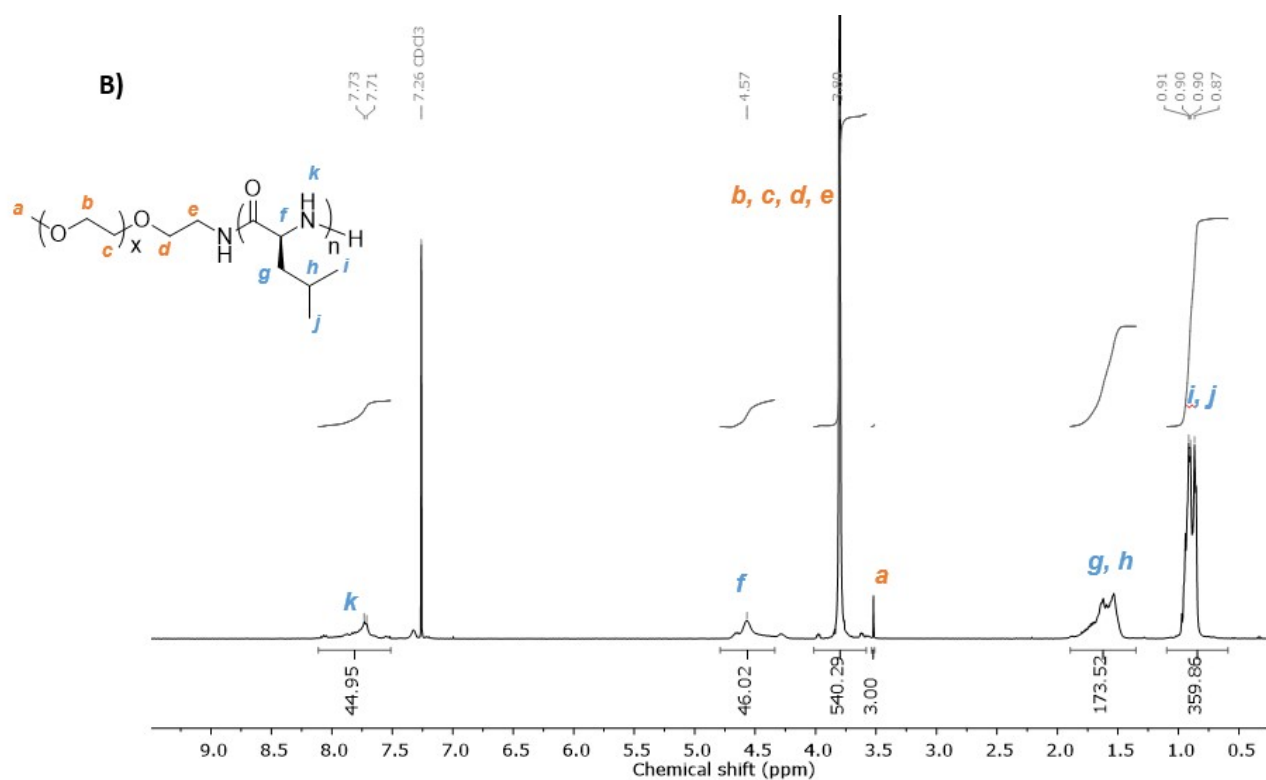


Figure S9. ^1H NMR of **PEG-*b*-PLeu₄₆** in CDCl_3 with TFA 30%

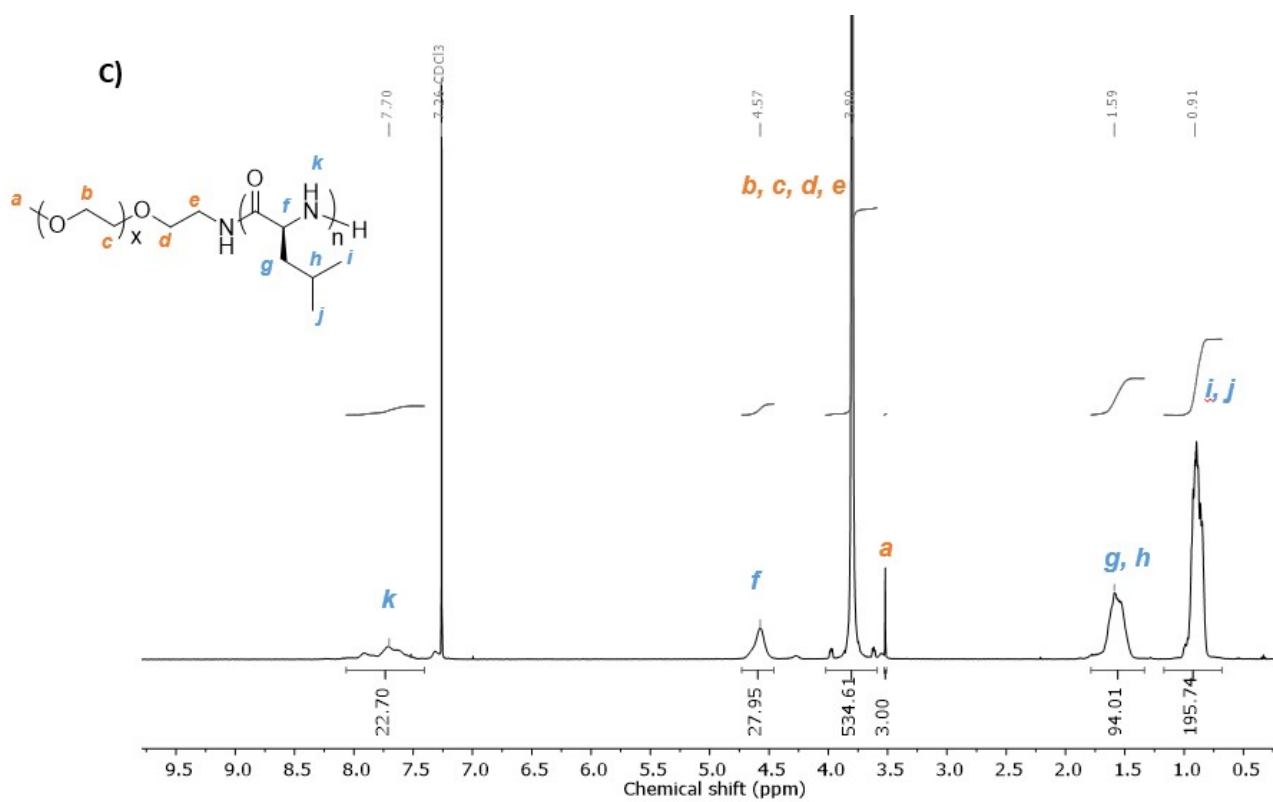


Figure S10. ^1H NMR of **PEG-*b*-PDLLeu₂₆** in CDCl_3 with TFA 30%.

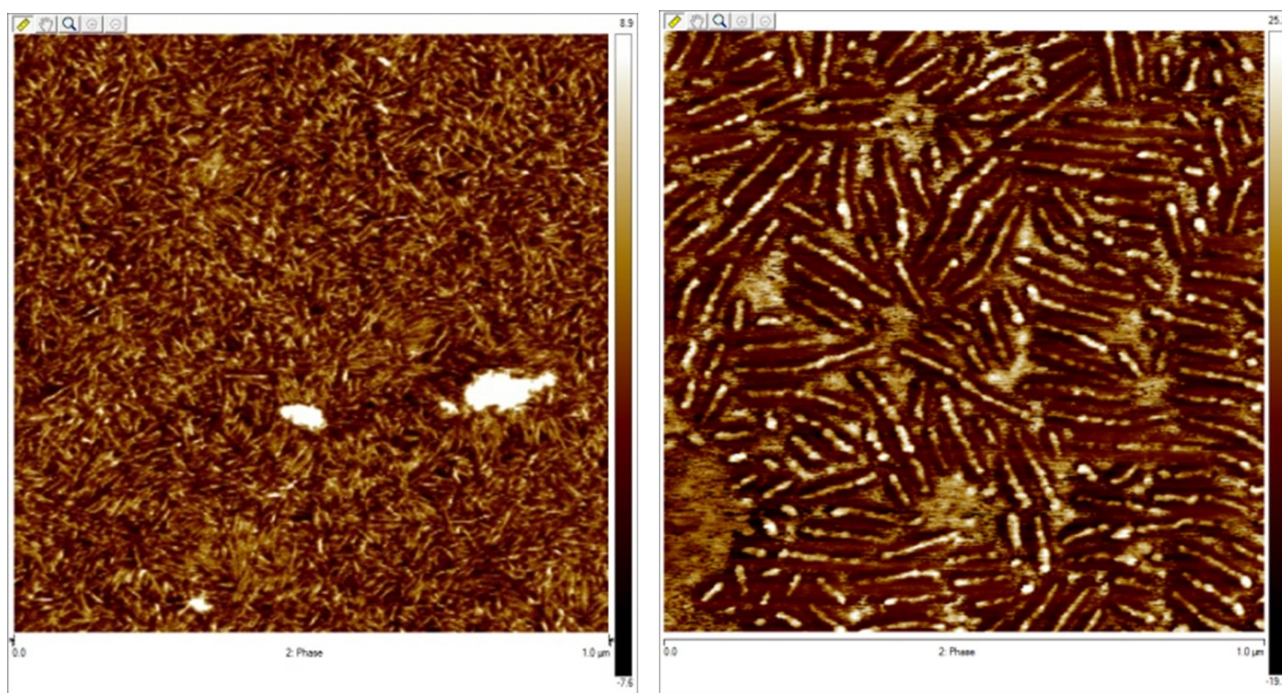


Figure S11: AFM imaging of the reaction mixture upon ROPISA performed at the same solid content ($\tau=7\%$) of **PEG-*b*-PBLG₂₂** (left) and **PEG-*b*-PLeu₂₆** (right). Note that the scale is the same for both images showing the difference in anisotropy brought by leucine monomer units.

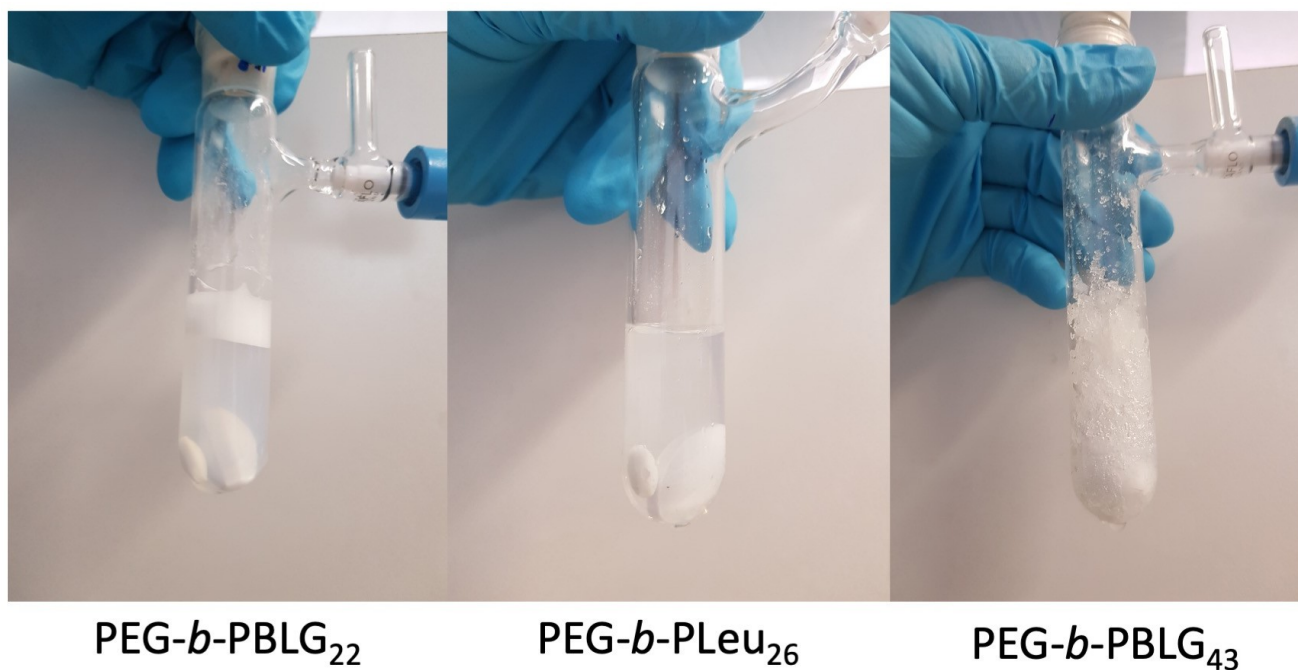


Figure S12. Pictures of the dispersion polymerization Schlenk tubes at the end of the ROPISA reaction, and before dialysis. In the case of **PEG-*b*-PBLG₄₃**, the aspect of the suspension is a soft (physical) gel.

SAXS data analysis

Here R_0 (Å) and L_0 (Å) designate respectively the median radius and median length of the polydisperse cylinders, σ_L and σ_R (no unit) being the standard widths of $\ln(L)$ and $\ln(R)$ distributions. The weight-average cylinder radius R_w (Å) and length L_w (Å) taking into account the particle polydispersity are then computed using formulas: $R_w = \langle R^4 \rangle / \langle R^3 \rangle = R_0 e^{1 + \frac{7}{2}\sigma_R^2}$ and $L_w = \langle L^4 \rangle / \langle L^3 \rangle = L_0 e^{1 + \frac{7}{2}\sigma_L^2}$. Some parameters were set at their theoretical values like the X-ray scattering length densities (SLD) calculated from the molecular formulas and mass densities of water, γ -benzyl-L-glutamate and L-leucine: $SLD_{\text{water}} = 9.43 \times 10^{-6} \text{ \AA}^{-2}$, $SLD_{\text{BLG}} = 11.5 \times 10^{-6} \text{ \AA}^{-2}$, and $SLD_{\text{Leu}} = 10.9 \times 10^{-6} \text{ \AA}^{-2}$. The X-ray contrast of PEO blocks was neglected owing to its hydrated state and SLD ($9.30 \times 10^{-6} \text{ \AA}^{-2}$) nearly equal to water. The particle volume fraction and the background intensity at high q were both let to vary by the fitting program. Depending on the samples, the whole SAXS curve could be approximately fitted on the whole q -range by a polydisperse cylindrical form factor, or just at the intermediate q -range, due to a low- q upturn ascribed to interacting or aggregating particles (bundles). The positions of the oscillations around $0.04\text{-}0.05 \text{ \AA}^{-1}$ corresponding approximately to π/R are qualitatively reproduced by the fits, although their amplitude can deviate from the experimental intensity curves, presumably due to polydispersity effect or to the experimental uncertainty (related to beam line collimation).

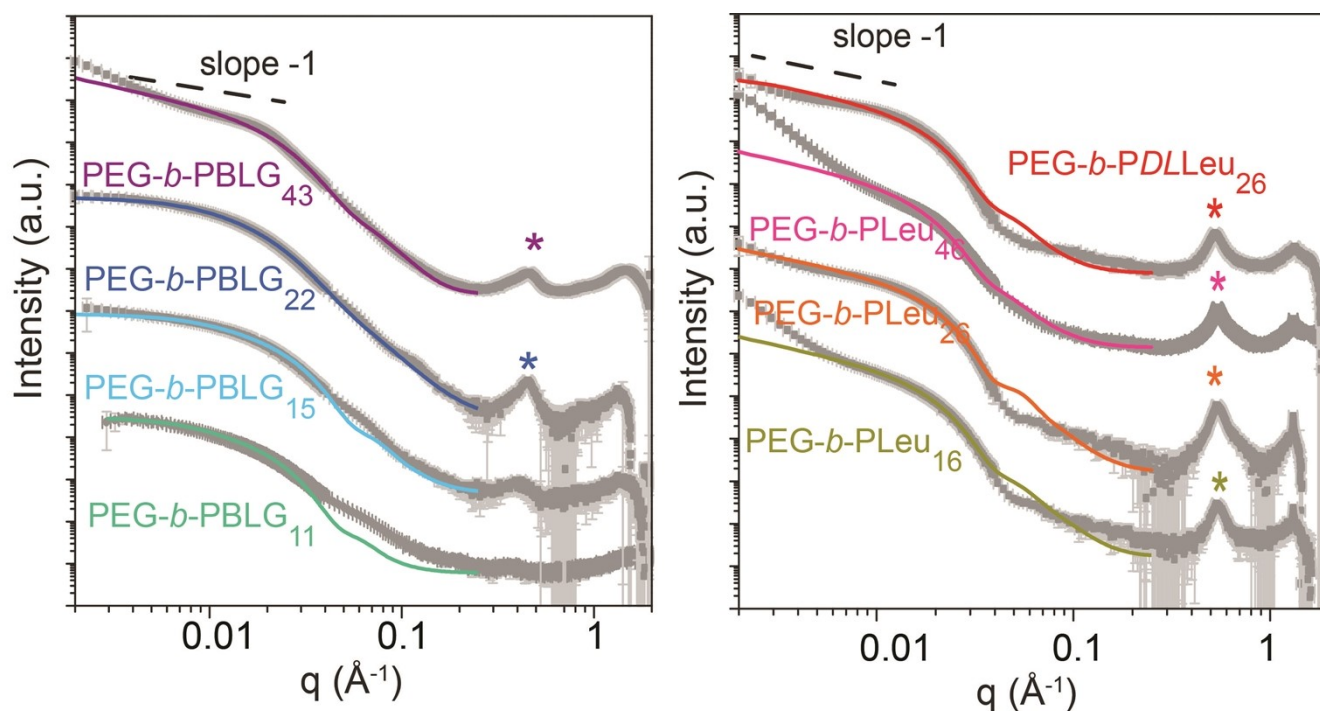


Figure S13. PEG-*b*-PBLG (left) and PEG-*b*-PLeu (right) series of copolymers analyzed by small-angle X-ray scattering (SAXS). Colored solid lines show the data fits obtained for each SAXS pattern using a polydisperse cylindrical model. For sake of clarity, two successive curves are offset by 2 decades in logarithmic scale ($\times 10^2$).

Table S1. Values calculated from the fits using the polydisperse cylinder model in SAXS analyses. The star is associated with a sample showing a significant amount of aggregation related for copolymer PEG-*b*-PBLG₄₃ and PEG-*b*-PLeu₄₆ to the formation of gels during ROPISA.

Copolymer	[M]/[I]	$R_0(\sigma_R) / R_w$ (Å)	$L_0(\sigma_L) / L_w$ (Å)	Aspect ratio ($L_w/2R_w$)
PEG- <i>b</i> -PBLG ₁₁	5	78(0.20) / 90	500(0.20) / 575	3.2
PEG- <i>b</i> -PBLG ₁₅	10	67(0.21) / 78	392(0.30) / 538	3.4
PEG- <i>b</i> -PBLG ₂₂	19	66(0.35) / 101	412(0.35) / 633	3.1
PEG- <i>b</i> -PBLG ₄₃	38	64(0.30) / 87	$5.2 \cdot 10^4(0.40) / 9 \cdot 10^4$	$\sim 100^*$
PEG- <i>b</i> -PLeu ₁₆	16	90(0.22) / 107	$4.4 \cdot 10^4(0.30) / 6 \cdot 10^4$	$\sim 60^*$
PEG- <i>b</i> -PLeu ₂₆	32	92(0.18) / 103.5	2484(0.25) / 3092	14.9
PEG- <i>b</i> -PLeu ₄₆	48	96(0.25) / 119	$3.9 \cdot 10^4(0.35) / 6 \cdot 10^4$	$\sim 50^*$
PEG- <i>b</i> -PDLLeu ₂₆	32	94(0.22) / 111	1400(0.28) / 1842	8.3

*For these samples exhibiting up-turn at low q vectors, the cylinder rod is only indicative because it cannot be determined accurately by the form factor fitting, therefore the calculated aspect ratio is just an order of magnitude.

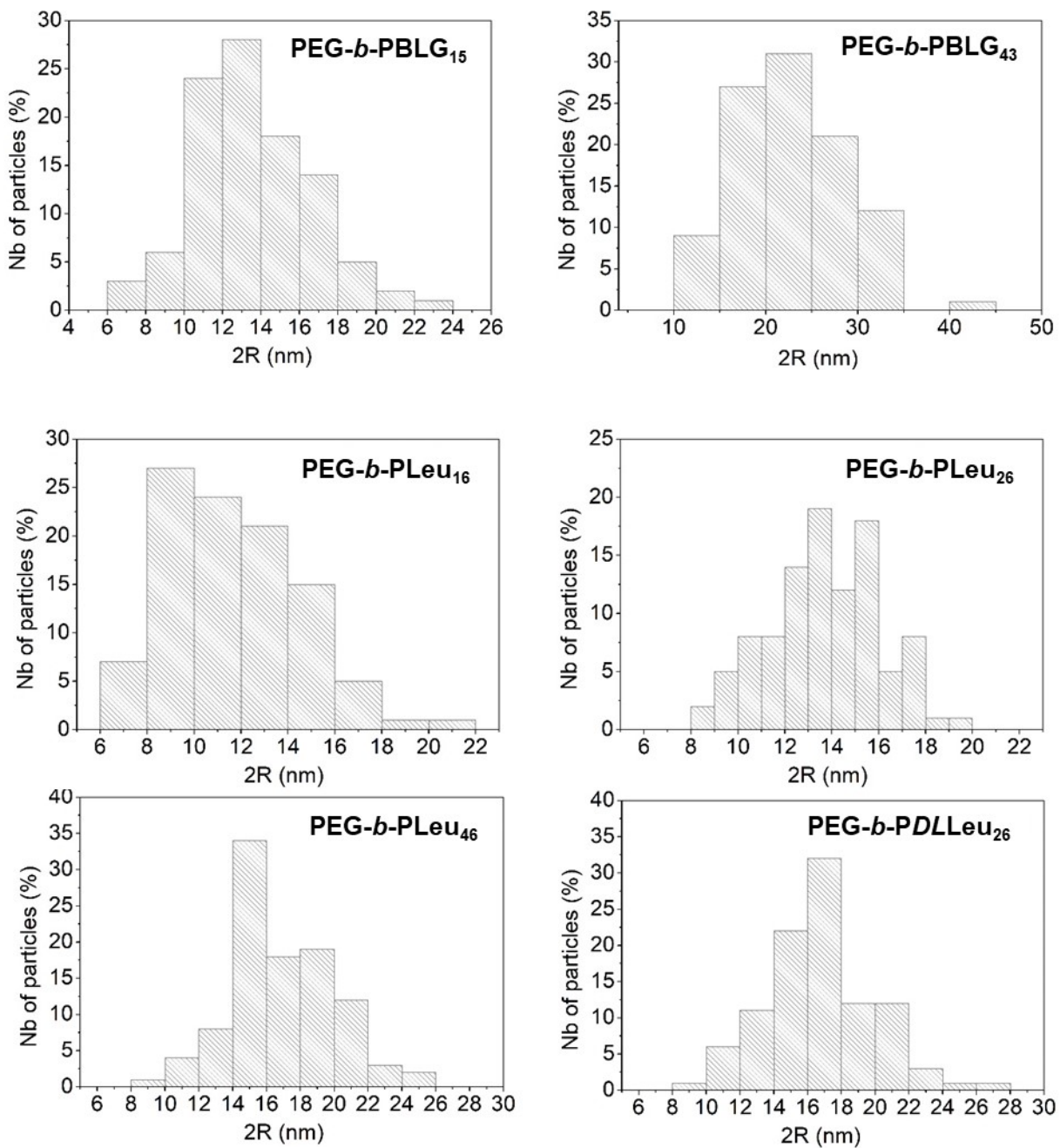


Figure S14. Diameter (2R) size distributions of the PEG-*b*-PBLG and PEG-*b*-PLeu nanoparticles obtained by analysis (imageJ) of 100 nanoparticles on a TEM image. PEG-*b*-PBLG₁₁ and PEG-*b*-PBLG₂₂ are not presented because the TEM image contrast and nanoparticles separation was not sufficient to give an accurate size distribution number.

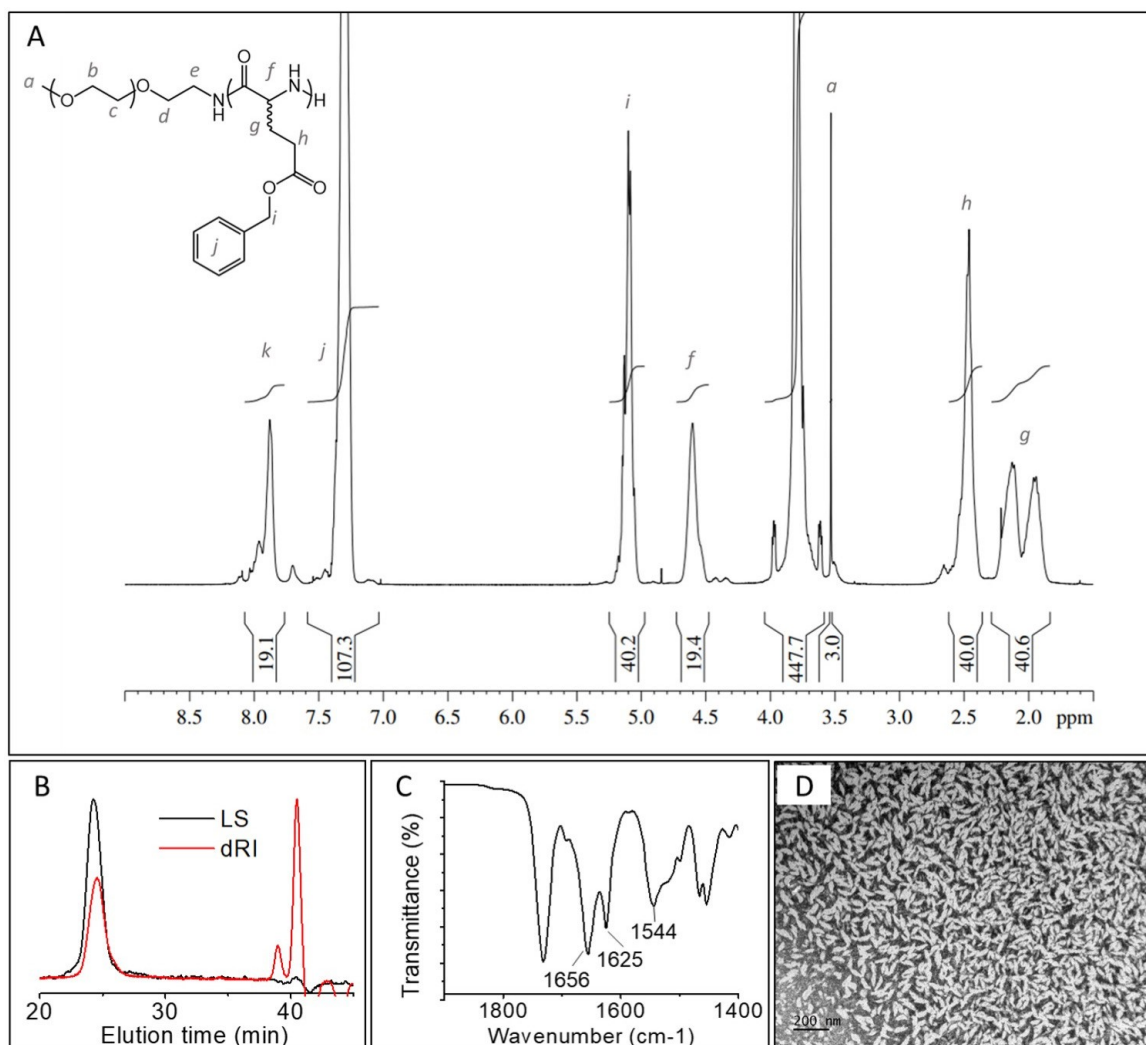


Figure S15. PEG-*b*-PBLDG₁₉: A) ¹H NMR spectra in CDCl₃ with TFA 15%; B) Steric exclusion chromatography analyzed in DMF (+1mg.mL⁻¹ LiBr); C) FTIR spectra showing the carbonyl stretching vibrations; D) TEM of the copolymer obtained by ROPISA and upon dialysis against milliQ water (negative staining using uranyl acetate).